ACS OMEGA

Open Access

http://pubs.acs.org/journal/acsodf

Article

Characterization of Water Vapor Sorption Performance and Heat Storage of MIL-101 (Cr) Complex $MgCl_2$, $LiCl/LaCl_3$ System for Adsorptive Thermal Conversion

Shang Liu, Ping Wu,* Guodong Fu, Shiping Zhang, Yanru Yang, Xiulan Huai, and Min Xu

Cite This: *ACS Omega* 2024, 9, 509−519

Read Online

ACCESS | Metrics & More | Article Recommendations

ABSTRACT: Adsorption heat conversion systems can provide heating and cooling across time and space in a more environmentally friendly way. Porous materials are potential candidates for water-based adsorption thermal conversion, in which a metal−organic framework (MOF) has a larger specific surface area and porosity than other porous matrices. However, many MOFs with high saturated adsorption capacity have great deficiencies in performance at low water vapor partial pressure, which hinder their application in adsorption thermal conversion. To improve the water vapor adsorption performance of MIL-101 (Cr), different contents of magnesium chloride, lithium chloride, and lanthanum chloride are mixed into MIL-101 (Cr) by an impregnation method. The properties and structures of the materials are characterized by XRD, SEM, nitrogen adsorption tests, water vapor adsorption tests, TG, FTIR, and so on. The results show that the saturated water vapor adsorption capacity of the sample impregnated with salt increases by 1.5−2.3 times, up to 2.24 g/g, compared with that of the unimpregnated sample. When the partial pressure of water vapor is 0.3, the adsorption capacity increases by 5.3−7.5 times and reaches 0.68 g/g at most. The maximum heat storage density of impregnated samples can be increased by 866 J/g. Impregnated $MgCl_2$ can greatly improve the adsorption and thermal conversion performance of MOF, and impregnated $MgCl_2$ and the proper amount of LiCl can further improve the performance of the material system. Our experiments show that the composite impregnation of magnesium chloride and the proper amount of lithium chloride can improve the application performance of the MOF materials in the adsorption thermal conversion process.

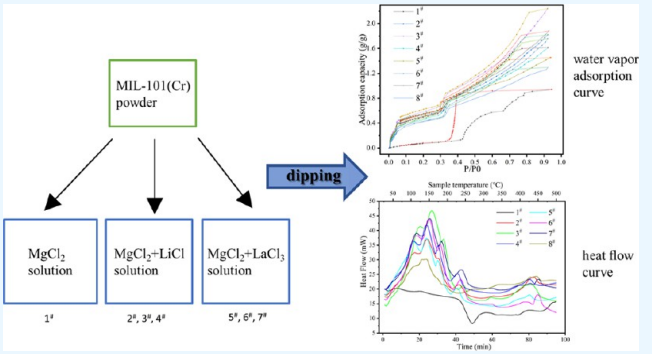

1. INTRODUCTION

The energy problem is one of the important challenges facing today's society. Energy storage and utilization across time and space are important methods to solve this problem, and it is also an urgent problem to be further solved at present. Heat storage is a more economical and efficient method of energy storage than electricity storage. Heat storage is divided into sensible heat storage, latent heat storage, and chemical reaction heat storage.[1] Chemical reaction thermal storage has the characteristics of high-energy storage density and a wide temperature range.[2] The adsorption heat pump is widely used in chemical reaction heat storage. It is an exothermic/endothermic system that utilizes adsorption/desorption between adsorbents and adsorbates and has been applied in industrial waste heat recovery,[3] seasonal heat storage,[4] refrigeration,[5] and so on. According to the adsorption process, adsorption heat pumps can be divided into three categories:[6] physical adsorption, chemical adsorption, and mixed adsorption. Ammonia,[7] acetone,[8] water vapor,[9] etc., are commonly used adsorbents in adsorption heat pumps. Because water is easily available and harmless, more adsorption heat pump systems choose water vapor as the adsorbate material. The commonly used adsorbents are mainly various porous materials, such as zeolite,[10] expanded vermiculite,[11] kaolin,[12] diatomite,[13] microporous aluminum phosphate,[14] and so on. They physically adsorb with water at lower temperatures and release heat, while they store heat by dehydration and heat absorption at higher temperatures.[1]

MOFs are a new kind of porous material developed in recent years. Compared with the porous materials mentioned above, MOF materials have the characteristics of large specific surface area, uniform pore structure distribution, and more micropore distribution, so they have better adsorption performance. MIL-

Received: August 14, 2023
Revised: November 19, 2023
Accepted: November 22, 2023
Published: December 26, 2023

101,[15] MIL-125,[16] MOF-505,[17] UIO-66,[18] and MOF-801[19] have been widely studied and paid attention to as adsorbent materials. Because of their excellent adsorption performance, MOFs have broad application prospects in adsorption thermal conversion. Harry Kummer[43] and others studied HKUST-1 and MIL-101 (Cr) as adsorption refrigerants and found that these materials have excellent adsorption properties. Jeremias et al.[41] studied the application of metal−organic framework UiO-66 and MIL-101 in adsorption thermal conversion. Henninger and others[42] studied ISE-1 and thought that this MOF could be used as an adsorbent for low-temperature heating and cooling applications. MIL-101 is a promising material for adsorption heat conversion because of its large specific surface area, high saturated water vapor adsorption capacity, and good water stability. Ehrenmann et al.[20] studied the performance of MIL-101 (Cr) as an adsorbent in an adsorption heat conversion system and found that its saturated adsorption capacity of water vapor can reach 1 g/g and its adsorption/desorption heat density can reach 2.557 kJ/g and 2.620 kJ/g. The disadvantage of MIL-101 (Cr) is that its water vapor adsorption capacity is not high at a low vapor pressure. Anupam Khutia et al.[21] prepared four kinds of nitro- or amino-functionalized MIL-101 (Cr). Although the saturated adsorption capacity of water vapor was increased, the adsorption capacity for a low water vapor partial pressure was hardly improved. George Akiyama et al.[17] prepared MIL-101 (Cr) with HCl, H_2SO_4, and HNO_3 instead of HF, which slightly increased the adsorption heat of the material but reduced the saturated adsorption capacity of MIL-101 (Cr) by 0.1 g/g. Existing studies have shown that the effect of increasing adsorption performance by changing the structure of MOF itself is limited, and it is difficult to improve the adsorption performance of materials under low water vapor partial pressure. Therefore, to further improve the water vapor adsorption performance and adsorption heat conversion performance of MIL-101 (Cr), it is imperative to prepare a composite system by compounding MIL-101 (Cr) with other adsorption heat conversion materials such as hydrate salt.[2]

Salt is a widely studied adsorbent material because of its low price and wide application temperature range. It can be used as adsorption heat conversion material at high temperatures,[21] medium temperatures,[22] and low temperatures.[23] Because the hydration/dehydration temperature of salt is almost the same as the adsorption/desorption temperature of the porous matrix, it is an effective means of preparing a composite system of salt and porous materials by impregnation. Yu et al.[25] prepared a consolidated composite matrix composed of activated carbon, LiCl, expanded graphite, and silica solution. Under the operating conditions of 85 and 40 °C, the heat storage efficiency of the system is 93% and the heat storage density is 874 kJ/kg. Emilie Courbon et al.[24] prepared silica gel loaded with $CaCl_2$ by continuous impregnation/drying, and its energy storage density reached 350 kWh/m^3. Vincenza Brancato et al.[27] prepared silicone foam filled with $MgSO_4 \cdot 7H_2O$. The results show that a good relationship seems to be established between foam and salt, and the dehydration/hydration ability of salt is not hindered by the foaming process. Hanane Ait Ousaleh et al.[44] combined $MgSO_4$ and $MgCl_2$ into a graphene matrix for medium and low-temperature heat storage. $MgSO_4$ and $MgCl_2$ composites achieved excellent energy storage densities of 1194.3 and 890 J/g, respectively. These studies show that the composite of porous materials and hydrated salts can significantly improve the heat storage capacity and adsorption capacity of a porous matrix at low temperatures.[3]

Similar to other porous materials, it is also an important method to improve the heat storage and adsorption properties of MOF materials by impregnation and other methods. Luis Garzón-Tovar et al.[28] prepared the mixture of $CaCl_2$ and UIO-66 by spray drying continuous flow method. The material has a heat storage density of 367 kJ kg^{-1}, and the composite is almost no deliquescence. Emilie Courbon et al.[26] doped LiCl into UIO-66 by the impregnation method, the saturated adsorption capacity of the composite reached 2.15 g/g and the heat storage density reached 900 kJ/kg. All of the above studies show that it is an effective means to combine MOF and salt to improve the water vapor adsorption performance and adsorption heat conversion performance of MOF materials. The dual-solvent method is an impregnation method developed from ordinary impregnation methods. Hanane Ait Ousaleh[26] and others prepared graphene containing $MgSO_4$ and $MgCl_2$ by dual-solvent method. Compared with the double solvent method, the traditional impregnation method has the advantages of simple operation and is suitable for large-scale industrial production. Therefore, we choose the impregnation method to obtain samples with a morphology closer to the practical application background. MIL-101 (Cr) can adsorb water vapor at room temperature, while salt can hydrate at room temperature. The working ranges of the two materials are similar. Salt has a better affinity with water at low partial pressure, and it is also expected to improve the water vapor adsorption performance of the MOF at low water pressure. The large pore volume of MIL-101(Cr) can accommodate more salt, which can greatly improve the water absorption. Therefore, we combine MIL-101 (Cr) with salt to improve the water vapor adsorption capacity and saturated water vapor adsorption capacity of MIL-101 (Cr) at low water vapor partial pressure and at the same time increase the heat storage density of MIL-101 (Cr). We chose $MgCl_2$, a salt with high heat storage density, low cost, and easy to obtain, to compound with MIL-101 (Cr). N'Tsoukpoe et al.[6] evaluated the applicability of 125 hydrated salts, among which LiCl and $LaCl_3$ have higher heat storage density than other salts. The article mentioned that the thermal storage density of $MgCl_2$ can reach 1252.8 kJ/g, $LaCl_3$ has a thermal storage density of 957.6 J/g, and LiCl has a thermal storage density of 1029.6 J/g, which is higher than other chloride salts. So we also attempted to impregnate LiCl or $LaCl_3$ at the same time as $MgCl_2$, exploring the effect of double salt impregnation. We also tried to impregnate another salt while impregnating $MgCl_2$, to further improve the water vapor adsorption capacity and adsorption heat conversion performance of the material system.

2. MATERIALS AND METHODS

2.1. Materials. The chemicals used in the experiment included terephthalic acid (99%), chromium nitrate (99%), *N*,*N*-dimethylformamide (DMF, 99.5%), hydrofluoric acid (40%), lithium chloride (99%), anhydrous magnesium chloride (99%), lanthanum chloride heptahydrate (99.99%), and anhydrous ethanol (99.7%), all of which are of commercial quality and can be used directly without further purification. All of the above chemicals were purchased from Beijing Honghu United Chemical Products Co., Ltd. Beijing, China.

2.2. Preparation of MIL-101(Cr) Composite $MgCl_2$, LiCl/$LaCl_3$ System. First, we prepared undoped MIL-101

https://doi.org/10.1021/acsomega.3c06004
ACS Omega 2024, 9, 509−519

Table 1. Sample Number (Based on Salt Content in Impregnation Solution)

sample number	$MgCl_2$ mass (g)	LiCl mass (g)	$LaCl_3 \cdot 7H_2O$ mass (g)	molar ratio
1 #	0	0	0	
2 #	5.00	0	0	
3 #	5.00	0.56	0	1:0.25:0
4 #	5.00	0.74	0	1:0.33:0
5 #	5.00	1.11	0	1:0.5:0
6 #	5.00	0	4.88	1:0: 0.25
7 #	5.00	0	6.50	1:0: 0.33
8 #	5.00	0	9.75	1:0: 0.5

(Cr)[28,29] according to the preparation method of Yan and others' published work and then impregnated the obtained products in solutions containing different amounts of salts. Each solution was obtained by mixing and stirring weighed salt and 20 mL of water, and the salt content in the solution is listed in Table 1. We hope that the salt concentration of the impregnation solution is high, so that as much salt can enter or adhere to MIL-101 (Cr) as possible, and it is necessary to ensure that it will not precipitate. Therefore, we chose 5 g salt with 20 mL water to prepare a salt solution with a mass concentration of 20%. After the salt solution was prepared, a 0.2 g MIL-101 (Cr) sample was added to each solution and stirred at the same time, so that it was uniformly mixed to obtain a uniform green suspension. After sealing the beaker and standing for 24 h, centrifuge and remove the supernatant and dry it in a 90 °C oven for 11 h. After drying, the sample was ground to obtain a green powder sample. We numbered the samples according to different preparation conditions, and the specific numbering is shown in Table 1.

3. RESULTS AND DISCUSSION

3.1. XRD Patterns of Samples. We use an X-ray diffractometer (XRD, Rigaku D/max2500X) to scan the diffraction spectrum of the sample, in which the X-ray source is Cu-Ka ray, the scanning step is 0.01, and the conventional 2 θ is used/θ (5−50). The X-ray diffraction pattern of the sample is shown in Figure 1. It can be seen from the figure that the XRD curve of the 1# sample is the same as the characteristic curve of MIL-101 (Cr) in the literature, and its characteristic peak corresponds to the simulation results,

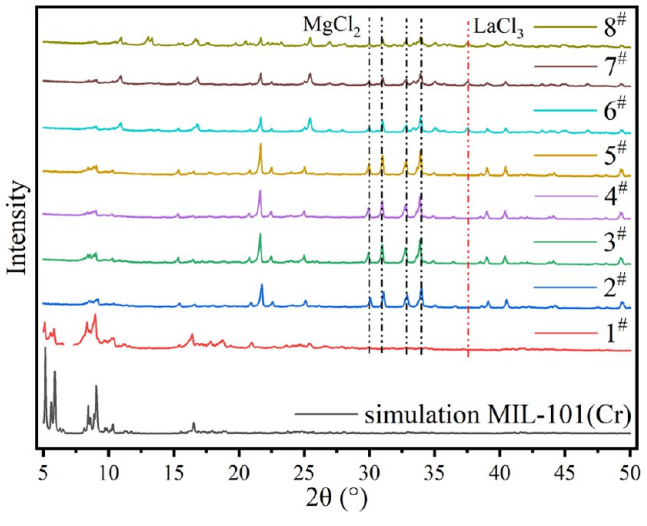

Figure 1. XRD patterns of samples.

indicating that the 1# sample is pure MIL-101 (Cr). After impregnation, only part of the characteristic peaks of MIL-101 (Cr) were retained, and the intensity of the peaks was weakened. This shows that salt impregnation leads to the change of pore structure and properties or the disorder of crystal structure.[30] The XRD images of all impregnated samples contain characteristic peaks of $MgCl_2$,[31] which indicates that the $MgCl_2$ crystal is attached to the surface or between particles of MIL-101 (Cr). There is no characteristic peak of LiCl in the samples impregnated with LiCl and $MgCl_2$, so we cannot judge the existence state of LiCl by XRD. The peak of $LaCl_3$ is also detected in the samples impregnated with LaCl and $MgCl_2$ at the same time, which indicated that $LaCl_3$ crystals also existed on the surface or between particles of the samples impregnated with $LaCl_3$.[4] The main peak in the range 22−26 is $MgCl_2 \cdot 6(H_2O)$. This may be due to the slight deliquescence of salt on the surface of the sample. Therefore, this peak can be found in samples 2−8. $MgCl_2$ and LiCl exist simultaneously in samples 3, 4, and 5, while $MgCl_2$ and $LaCl_3$ exist simultaneously in samples 6, 7, and 8. We believe that the presence of lithium chloride enhances the deliquescence of samples, thus enhancing the peak of magnesium chloride hexahydrate. However, the crystal size of lanthanum chloride is larger, which may weaken the deliquescence of samples.

3.2. SEM Images of the Samples MIL-101 (Cr) and MIL-101 (Cr, Mn). We used scanning electron microscopy (FESEM, Zeiss supra 55) to characterize and analyze the microscopic particle morphology of the prepared samples. Before the observation, we sprayed gold onto the samples. Figure 2 shows SEM images of eight samples. As can be seen from Figure 2, the particles of MIL-101(Cr) have a regular octahedral structure and a smooth surface. After impregnation, the sample still basically keeps an octahedral structure, but burrs and pits appear on the surface. This is also the reason for the weakening of the MIL-101 (Cr) characteristic peak in the XRD results of samples. It can be observed that most of the particles condense with salt, and the attached salt can also be observed on the scattered particle surface, which is consistent with the results of XRD.

At the same time as morphology characterization, we carried out a microelemental analysis to observe the proportion and distribution of each element in the sample. Although the impregnation method is suitable for large-scale industrial production and the method is simple, the samples obtained by it may have uneven ion distribution. Therefore, we hope to determine whether the relative content of metal ions in the sample is basically consistent with that in the impregnation solution by the EDX test. Because EDS cannot detect the signal of the Li element, we only carried out relevant tests on samples 6−8. Figure 3 shows the EDS spectra of samples 6−8. The impregnation solution of samples 6−8 is a mixed solution

https://doi.org/10.1021/acsomega.3c06004
ACS Omega 2024, 9, 509−519

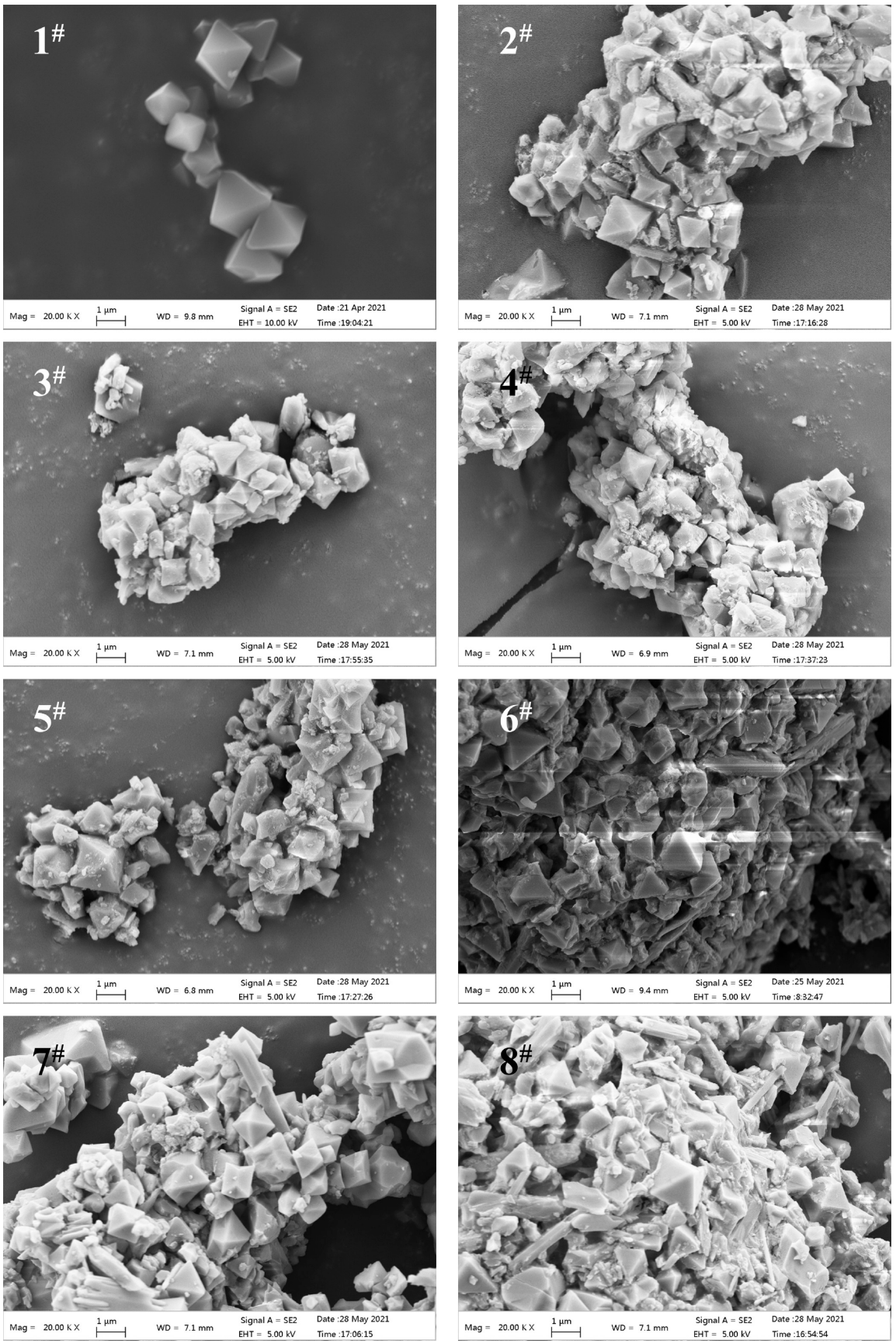

Figure 2. SEM images of the samples.

https://doi.org/10.1021/acsomega.3c06004
ACS Omega 2024, 9, 509−519

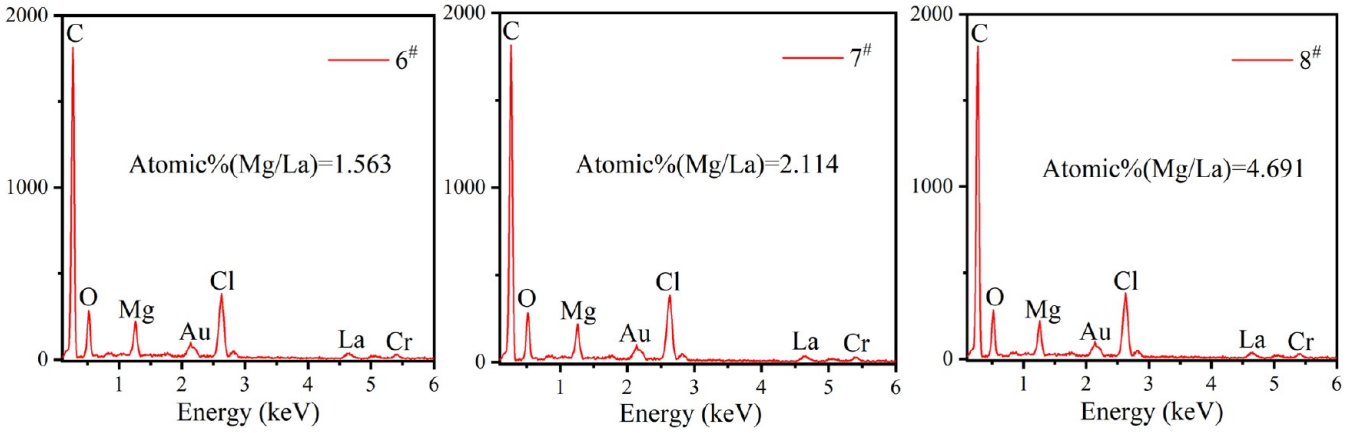

Figure 3. EDS spectra of the samples.

of $MgCl_2$ and $LaCl_3$. Mg, Cl, and La elements can be detected in the energy spectrum. The atomic ratio of Mg to La in samples 6−8 increased with the increase of the molar ratio of Mg to La in the impregnation solution, which indicated that the salt content in the impregnation sample was directly related to the salt concentration in the impregnation solution.

3.3. FTIR Spectra and the Raman Spectra of the Samples MIL-101 (Cr, Mn) and MIL-101 (Cr). We used FTIR (Lambda FTIR-7600) to test the mid-infrared absorption spectrum of the sample. KBr was used as the background in the test. The spectral resolution is 2 cm^{-1}, and the scanning range is 400−4000 cm^{-1}. All samples showed a pattern similar to MIL-101 (Cr), which is consistent with that reported in the literature.[32] MIL-101 (Cr) has a moderate absorption peak at the wave number of 587 cm^{-1}, which is the stretching vibration peak of (Cr−O).[33] The peaks of samples impregnated with the salt move to a high wave number, and the peak width becomes larger. This indicates that the chemical environment of the Cr−O bond in the impregnated samples may change. Compared with the unimpregnated sample, the impregnated sample has a new characteristic peak at 2276 cm^{-1}, which is the characteristic peak of $MgCl_2$.[34] This indicates the presence of $MgCl_2$ in the impregnated sample. A new peak appeared in the impregnated sample at 3242 cm^{-1}, which, like the peak at 3423 cm^{-1}, is caused by the stretching vibration of the H−O bond.[35] Compared with MIL-101 (Cr), the impregnated sample increased the way of absorbing water vapor, and the connection mode between adsorbed water and the sample has increased. After impregnation, there are small peaks at 2925 and 2853 cm^{-1}, which may be the peaks of liquid water molecules.[35] This shows that MIL-101 (Cr) is deliquescent more easily by salt impregnation than before impregnation (Figure 4).

3.4. N_2 Adsorption Isotherms of the Samples. The sample was degassed at 120 °C for 6 h by using the vapor adsorption and specific surface pore size analyzer (BSD-PMV), and then the nitrogen adsorption curve of the sample was measured at 77.3 K constant temperature, and then the specific surface area and pore size distribution of the sample were obtained. Figure 5 shows the nitrogen adsorption curve of the sample. It can be seen from the figure that the nitrogen adsorption curve of MIL-101 (Cr) is a type I curve, and no obvious hysteresis loop is observed. The nitrogen adsorption curve of the sample impregnated with salt solution changed to a type II curve, and an H3-type hysteresis loop appeared. The change of the hysteresis loop of the nitrogen adsorption curve

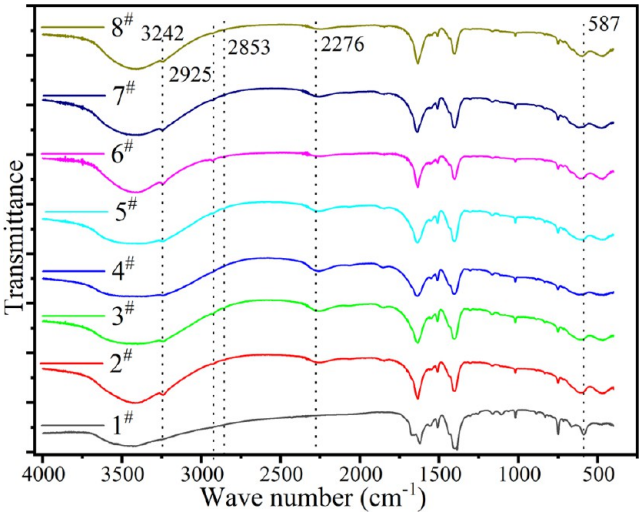

Figure 4. FTIR spectra of MIL-101 (Cr) and MIL-101 (Cr, Mn).

of impregnated samples shows that the proportion of mesopores in samples increases after impregnating salt solution, and the pore distribution is more dispersed than that without impregnation. Table 2 lists the BET-specific surface area and BJH average pore size of each sample. It can be seen from the table that the BET-specific surface area of the impregnated sample decreases greatly and the average pore size increases slightly, which also shows that the mesopore ratio of the impregnated sample increases.

Figure 6 shows the pore size distribution of the sample. It can be found from the figure that the pores of MIL-101 (Cr) are distributed at 2 nm, while the impregnated samples have a mainly distributed pore size around 2 nm, which leads to the increase of pore ratio in the samples and then leads to the change of hysteresis loop in the nitrogen adsorption curve. The three chloride salts used in the experiment do not exist as separate ions in an aqueous solution, The Cl^--H_2O cluster size is about 0.28−0.32 nm,[36] the La^{3+}-H_2O cluster size is about 0.39 nm,[37] and the Mg^{2+}-H_2O cluster size and the Li^+-H_2O cluster size are about 0.2 nm,[38] which are all smaller than the 2 nm pore size of the sample without impregnation. Therefore, the pore size of MIL-101 (Cr) may be filled when the specific surface area of the sample is greatly reduced. The pore size distribution of samples impregnated with La increases to a small peak near 4 nm. Combined with the results of SEM and

https://doi.org/10.1021/acsomega.3c06004
ACS Omega 2024, 9, 509−519

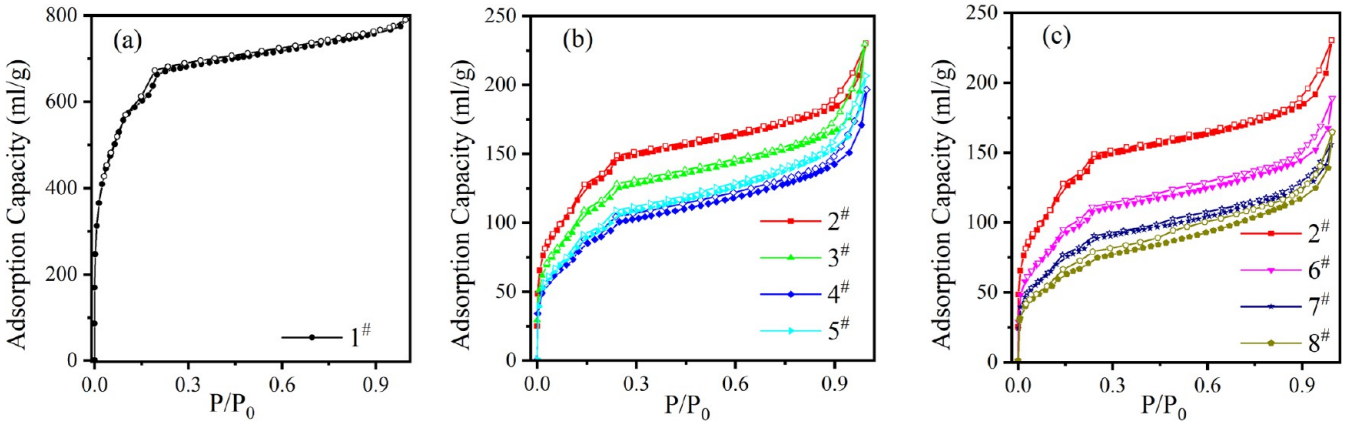

Figure 5. N_2 isotherms of unimpregnated (a), impregnated magnesium chloride, lithium chloride (b), and impregnated magnesium chloride, green lanthanum (c).

Table 2. Variable Specific Surface Areas of the Samples

adsorbent	BET-specific surface area (m^2/g)	the average pore diameter of BJH desorption (nm)
1 #	2119.7	2.4
2 #	479.1	2.9
3 #	416.3	3.4
4 #	334.0	3.4
5 #	349.6	3.5
6 #	355.7	3.1
7 #	292.5	3.2
8 #	250.9	3.6

XRD, 4 nm pores may be formed between salts attached to the surface of MOF.[5]

3.5. Water Vapor Isotherms of the Samples. Steam adsorption and a specific surface pore size analyzer (BSD-PMV) were used to measure the water vapor adsorption curve of the sample at 25 °C. Before the test, the sample was degassed at 120 °C for 6 h. After degassing, we put the sample in the instrument, set the water vapor adsorption temperature (25 °C), and input the saturated vapor pressure at this temperature. The instrument will automatically test the adsorption capacity of samples under different vapor pressures, so we need to wait for the instrument to finish the test. Figure 6 shows the water vapor adsorption curve of the sample. For unimpregnated samples, only MIL-101 (Cr) plays an adsorption role; therefore, the whole adsorption process is physical adsorption. For impregnated samples, MIL-101 (Cr) and impregnated salt are involved in the adsorption process; therefore, water vapor adsorption can be divided into two parts: physical adsorption and chemical adsorption. It can be seen from Figure 7 that the saturated water vapor adsorption capacity of the sample impregnated with salt is higher than that of pure MIL-101 (Cr). The saturated adsorption capacity of each sample is given in Table 3. In Figure 6, when $P/P_0 < 0.1$, all impregnated samples have a sudden rising curve, which is mainly due to the hydration reaction between impregnated salt and water vapor. The desorption curve of the impregnated sample terminates at the highest part of this rising curve, which also shows that the adsorption process is mainly participated by salt, and the sample is chemisorbed at this stage, so it is difficult to desorb by physical means. Figure 6b shows the water vapor adsorption curve of $MgCl_2$. The water vapor adsorption isotherms of impregnated samples are very similar to those of pure salts, and the steps correspond to the formation of crystalline hydrates at low P/P_0 and then the absorption of water by deliquescent salts at higher P/P_0 due to deliquescence and absorption of salt hydrates, which indicates that most of the water adsorbed by impregnated samples comes from impregnated salts.[39,40] When we prepare samples, the amount of magnesium chloride in the impregnation

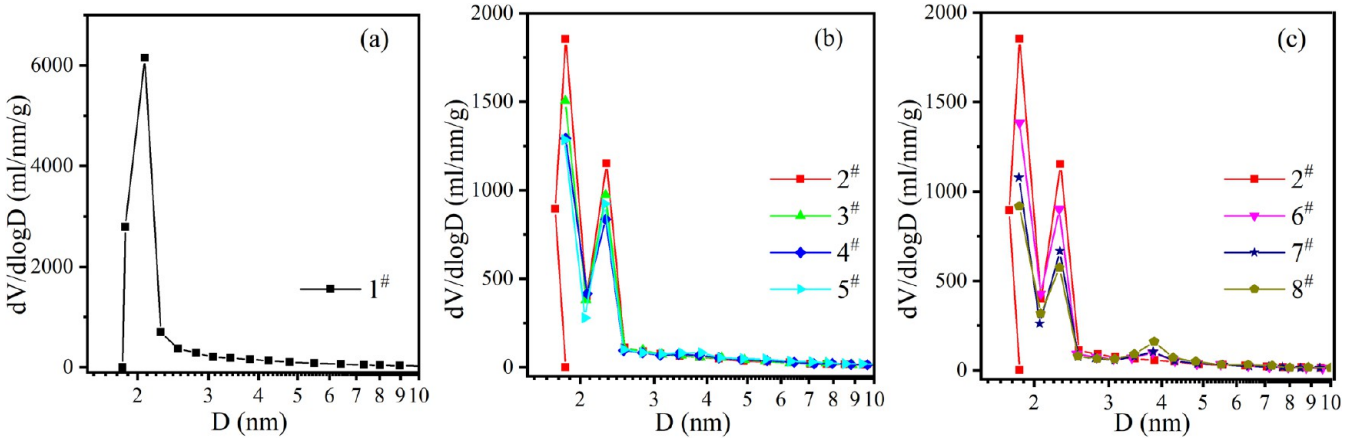

Figure 6. Pore size distribution of unimpregnated (a), impregnated magnesium chloride, lithium chloride (b), and impregnated magnesium chloride, green lanthanum (c).

https://doi.org/10.1021/acsomega.3c06004
ACS Omega 2024, 9, 509−519

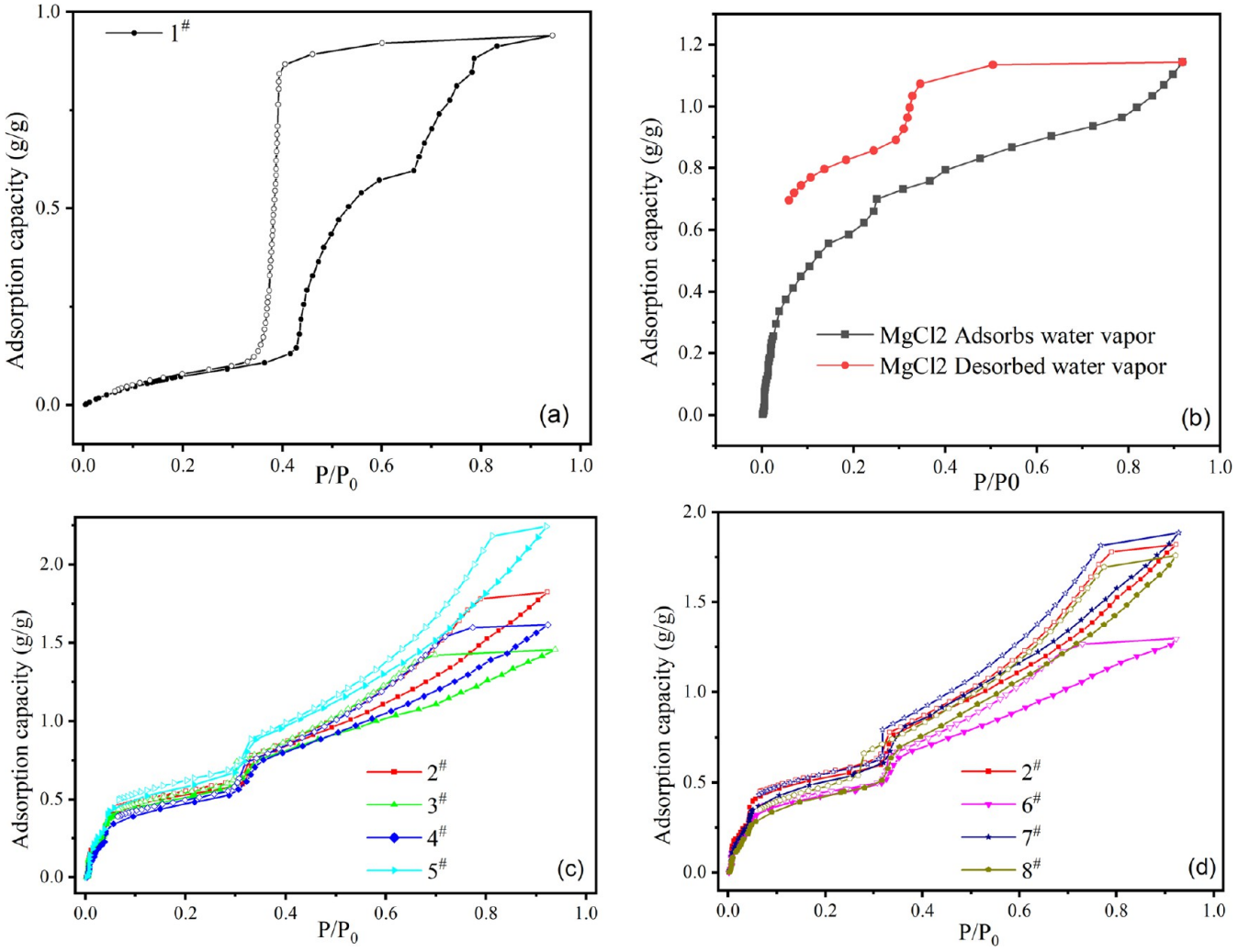

Figure 7. Water vapor isotherms of unimpregnated (a), water vapor isotherms of $MgCl_2$ (b), impregnated magnesium chloride, lithium chloride (c), and impregnated magnesium chloride, green lanthanum (d).

Table 3. Maximum Adsorption Capacity and the α Value of Samples

adsorbent	saturated adsorption capacity (g/g)	adsorption capacity at P/P_0 = 0.3 (g/g)	α
1 #	0.94	0.09	0.51
2 #	1.82	0.58	0.46
3 #	1.46	0.59	0.34
4 #	1.61	0.55	0.40
5 #	2.24	0.68	0.49
6 #	1.30	0.48	0.36
7 #	1.88	0.59	0.46
8 #	1.76	0.49	0.48

solution used for each sample is the same, but different amounts of the second salt are added. Therefore, the relative content of $MgCl_2$ in the impregnation solution of samples 3 and 4 will be lower than that of the impregnation solution of sample 2, and the content of $MgCl_2$ in these two samples is higher than that of LiCl. For the surface of the sample, the number of water molecules that lithium chloride can bind to is lower than that of magnesium chloride, and the hydrates formed at this time may block the pores of the MIL, preventing more water vapor from entering the pores or coming into contact with more salts. Therefore, the adsorption capacity of samples 3 and 4 is lower than that of sample 2. The significant increase in the adsorption capacity of sample 5 may be because the amount of salt in the impregnation solution of sample 5 is the highest compared with samples 3 and 4, and then, there are more salts on the surface. For sample 6, compared with sample 2, part of $MgCl_2$ was replaced by $LaCl_3$ with a larger molecular diameter, which led to the decrease of the total amount of salts on the surface of the sample that could participate in hydration, and the formed hydrate also led to the blockage of the pores of MIL-101. According to our current experimental results, we think that the further increase of LiCl content may contribute to the improvement of adsorption capacity. When $P/P_0 > 0.8$, the adsorption capacity of MIL-101 (Cr) for water vapor hardly increased, but the adsorption capacity of impregnated samples still increased at this stage. This shows that when $P/P_0 > 0.8$, MIL almost no longer adsorbs water vapor, and the increase of adsorption capacity in impregnated samples is due to the adsorption of water vapor by impregnated salts. Gordeeva[18] et al. studied the process of water adsorption by salt. Their research showed that hydrated salt adsorbed water vapor to form crystal hydrate at low P/P_0, and hydrated salt continued to adsorb water vapor at high P/P_0 and then deliquesced to form salt aqueous solution. For our sample, according to the results of pore size analysis, the

https://doi.org/10.1021/acsomega.3c06004
ACS Omega 2024, 9, 509−519

volume of adsorbed water vapor has far exceeded the specific pore volume of the composite material. Therefore, we think that most of the adsorbed water after impregnating the sample $P/P_0 > 0.8$ comes from the excessive water vapor adsorbed by salt, which leads to deliquescence and saline solution. All samples have obvious hysteresis loops at $0.4 < P/P_0 < 0.8$, which indicates that the samples adsorb water vapor by capillary action at this stage.[41] The hysteresis loop of the impregnated sample is much reduced. According to the experimental results of nitrogen adsorption, the average pore size of the impregnated sample increases, which may lead to the decrease of the resistance caused by the capillary effect in the water vapor desorption stage, resulting in the decrease in the hysteresis loop. The decrease in the hysteresis loop may also be due to the decrease in pores and the increase in adsorption capacity, so it seems that the hysteresis loop caused by pore water absorption also becomes smaller. Compared with the samples impregnated with different impregnating solutions, the saturated adsorption capacity of the samples impregnated with $MgCl_2$ and $LaCl_3$ did not increase significantly compared with the samples impregnated with $MgCl_2$ alone. However, the increase in saturated adsorption capacity was greatest for the samples immersed in the most LiCl, suggesting that further addition of LiCl after addition of $MgCl_2$ is a more effective means than further addition of $LaCl_3$.[6]

According to Canivet, the change of α can be used to characterize the adsorption capacity of water vapor under the low partial pressure of materials. α is the ratio of pressure to saturated vapor pressure at room temperature when the adsorbed substance reaches half of the maximum adsorption capacity (P/P_0). When α is less than 0.05, this indicates that the material has strong water vapor adsorption capacity at low partial pressure. When α is greater than 0.45, the water vapor adsorption ability of the material is weak under low partial pressure.[32] The smaller the α, the stronger the adsorption capacity of the material at lower water vapor partial pressure. Table 3 lists the adsorption capacity and α value of the sample at a partial pressure of 0.3. It can be seen from the table that the α value of the samples impregnated with salt solution has been improved to some extent, and the water vapor adsorption capacity of the impregnated samples under lower vapor pressure has also been improved. For samples impregnated with the same salt solution, the lower the concentration of the salt solution, the smaller the value of α after impregnation, indicating that the material is relatively hydrophilic. The sample with the largest LiCl content has the highest water vapor adsorption capacity and the largest saturated adsorption capacity at low water pressure, while the addition of $LaCl_3$ has no obvious improvement compared with the impregnation of $MgCl_2$.[7]

3.6. TG Curves of the Samples. Samples subjected to water vapor adsorption−desorption experiments were placed in a synchronous thermogravimetric analyzer (TGA, PerkinElmer STA8000), and their mass change curves were measured at a temperature range of 30−500 °C and a heating rate of 5 °C/min, as shown in Figure 8. As can be seen from Figure 8, all of the impregnated samples can observe a significant decline in quality before 200 °C. At 200 °C, the remaining mass of each sample accounts for the initial mass, as shown in Table 4, and the mass of impregnated samples decreases by 30−40%. For impregnated samples, the hydrated salt in the sample removes the water bound by adsorption at this temperature. After 200 °C, the quality change of impregnated samples tends to be stable, while that of unimpregnated samples changes greatly. Compared with 200 °C, the final mass of unimpregnated samples decreased by 56.1%, and that of impregnated samples decreased by about 30%. Figure 8 shows a DTG curve of the sample during heating. For unimpregnated samples, the peak at about 50 °C represents the desorption of adsorbed water on the samples. The peak between 200 and 350 °C represents the decomposition of free organic ligands and the OH/F group and the decomposition of terephthalic acid. Peaks above 400 °C represent the decomposition of the organic ligand chain of the sample itself. For the impregnated sample, the DTG peak at 200 °C is less than that of the unimpregnated sample, which may be attributed to the salt impregnated in MOF.

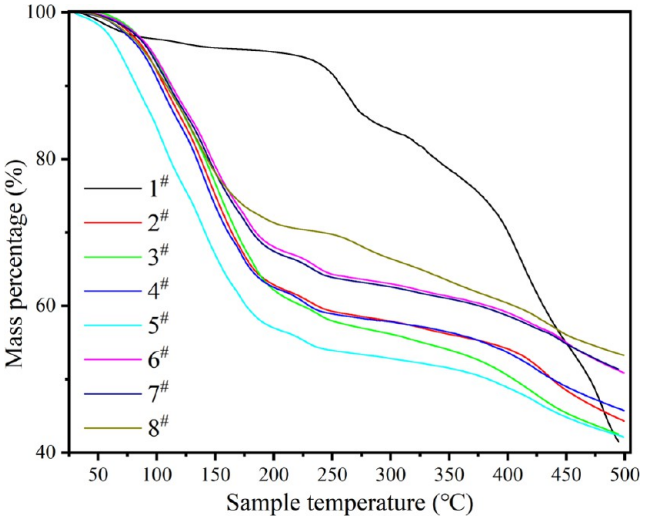

Figure 8. Thermogravimetry of samples.

Table 4. Remaining Mass of Samples Heated to Different Temperatures (Expressed in Percentage)

adsorbent	200 °C (%)	500 °C (%)
1 #	94.6	41.5
2 #	62.8	44.2
3 #	62.1	42.4
4 #	62.5	47.0
5 #	56.9	42.5
6 #	68.0	50.9
7 #	67.4	51.3
8 #	71.3	53.1

The heat flux curve during the heating process of the sample is shown in Figure 9. It can be seen from the figure that the heat flux peaks of samples after impregnation are mainly distributed before 200 °C, 200−250 °C, and after 400 °C. The peak before 200 °C comes from the dehydration and endothermic process of the salt. The peak shape of the heat flux curve of DTG also corresponds to the main peak position of DTG, which indicates that the main mass change of samples also appears at the corresponding temperature during dehydration and decomposition. From this heat flow curve, we calculated the heat storage density of each sample, which is listed in Table 5. Because the samples we used for thermogravimetric experiments have undergone the water vapor adsorption−desorption test, the water contained in the thermogravimetric samples is only the water adsorbed in the

https://doi.org/10.1021/acsomega.3c06004
ACS Omega 2024, 9, 509−519

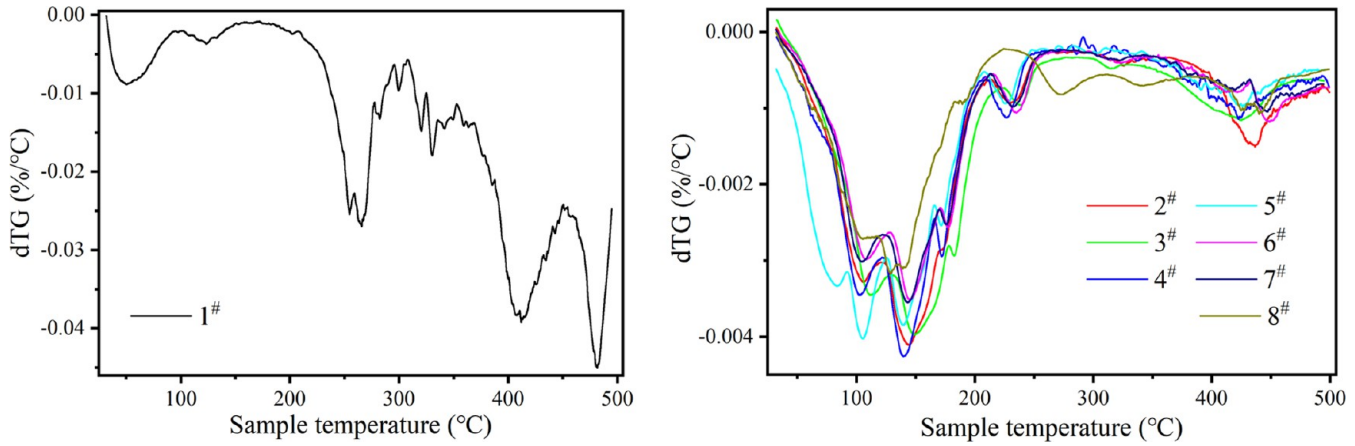

Figure 9. Differential thermogravimetry curve of samples.

Table 5. Heat Storage Density during Sample Dehydration (<200 °C)

sample number	2 #	3 #	4 #	5 #	6 #	7 #	8 #
ΔH (J/g)	818.9	810.1	866.1	817.5	712.5	707.6	820.8

chemical adsorption process. Therefore, the heat storage density calculated from this heat flow curve is only the heat storage density in chemisorption. It can be seen from the table that the increased chemisorption heat storage density of impregnated samples is about 800 J/g, and the chemical heat storage density of double salt components is not improved compared with that of single salt components. The increased thermal storage density of two-component salt-impregnated samples impregnated with LiCl and $MgCl_2$ is obviously higher than that of single salt-impregnated samples impregnated with $MgCl_2$, but the increased thermal storage density of two-component salt-impregnated samples impregnated with $LaCl_3$ and $MgCl_2$ is almost unchanged or even decreased compared with single salt impregnated samples impregnated with $MgCl_2$ (Figure 10).[8]

4. CONCLUSIONS

The water vapor adsorption and heat storage properties of the MIL-101 (Cr) complex salt system were studied by an impregnation method with different concentrations of $MgCl_2$, LiCl, and $LaCl_3$ doped into MIL-101 (Cr). Generally speaking, the addition of salt makes the saturated adsorption capacity of the system greatly increased compared with pure MIL-101 (Cr), which makes the saturated adsorption capacity more than doubled and makes the system more compatible with water vapor. At 25 °C and P/P_0 = 0.3, the water vapor adsorption capacity increased by up to five times to 0.68 g/g, which greatly increased the service performance of the system in a low water vapor partial pressure environment. Our experimental results show that compared with $MgCl_2$−$LaCl_3$ composite impregnation, $MgCl_2$−LiCl composite impregnation can improve the water vapor adsorption capacity of the system more significantly. Compared with single-component impregnation, multicomponent impregnation can improve the water vapor adsorption capacity of samples under low water pressure, but it will make the materials relatively hydrophobic. The results of TGA showed that the thermal storage density of the impregnated samples increased obviously, and the chemical thermal storage density of the impregnated samples with $MgCl_2$ and the proper amount of LiCl increased the most, which could increase by 866 kJ/mol. Nitrogen adsorption experiments show that impregnation can reshape the pore structure of MOF materials and increase the mesoporous content in the system. The results of XRD and FTIR showed that the impregnation did not change the structure of MIL-101 (Cr), and it increased the adsorption mode of water vapor. Our experiments show that the sample containing both $MgCl_2$ and LiCl in the impregnation solution has the highest water vapor adsorption capacity, saturated water vapor adsorption capacity, and heat storage density under low partial pressure. This composite material greatly improves the adsorption capacity and heat storage density of MIL-101 (Cr) under low water vapor partial pressure, and its preparation method is simple, which is suitable for large-scale industrial production and is expected to become a candidate material for low-temperature heat storage.

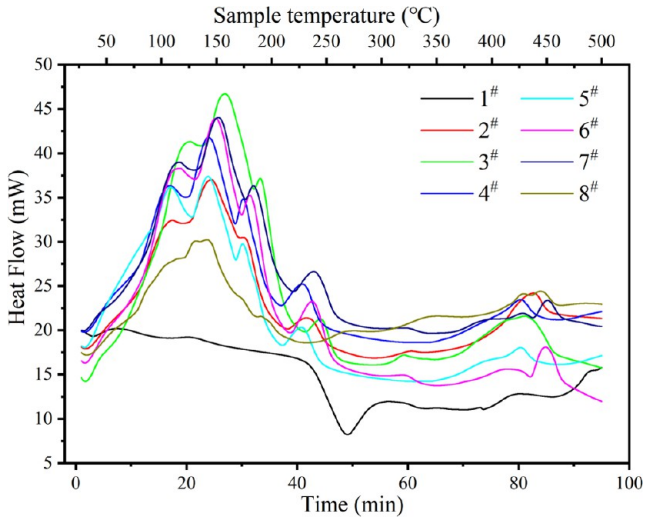

Figure 10. Differential thermogravimetry curve of samples.

https://doi.org/10.1021/acsomega.3c06004
ACS Omega 2024, 9, 509−519

■ ASSOCIATED CONTENT

Data Availability Statement

The data that support this study will be shared upon reasonable request by the corresponding author.

■ AUTHOR INFORMATION

Corresponding Author

Ping Wu − *Beijing Key Laboratory for Magneto-Photochemical Composite and Interface Science, School of Mathematics and Physics, University of Science and Technology Beijing, Beijing 100083, China;* orcid.org/0000-0002-7797-0828; Email: pingwu@sas.ustb.edu.cn

Authors

Shang Liu − *Beijing Key Laboratory for Magneto-Photochemical Composite and Interface Science, School of Mathematics and Physics, University of Science and Technology Beijing, Beijing 100083, China*

Guodong Fu − *Beijing Key Laboratory for Magneto-Photochemical Composite and Interface Science, School of Mathematics and Physics, University of Science and Technology Beijing, Beijing 100083, China*

Shiping Zhang − *Beijing Key Laboratory for Magneto-Photochemical Composite and Interface Science, School of Mathematics and Physics, University of Science and Technology Beijing, Beijing 100083, China*

Yanru Yang − *Beijing Key Laboratory for Magneto-Photochemical Composite and Interface Science, School of Mathematics and Physics, University of Science and Technology Beijing, Beijing 100083, China*

Xiulan Huai − *Institute of Engineering Thermophysics, Chinese Academy of Sciences, Beijing 100190, China*

Min Xu − *Institute of Engineering Thermophysics, Chinese Academy of Sciences, Beijing 100190, China;* orcid.org/0000-0003-4033-9204

Complete contact information is available at: https://pubs.acs.org/10.1021/acsomega.3c06004

Notes

The authors declare no competing financial interest.

■ ACKNOWLEDGMENTS

This work was financially supported by the National Natural Science Foundation of China (No. 51836009).

■ REFERENCES

(1) André, L.; Abanades, S.; Flamant, G. Screening of thermochemical systems based on solid-gas reversible reactions for high temperature solar thermal energy storage. *Renewable Sustainable Energy Rev.* **2016**, *64*, 703−715.

(2) Yan, J.; Zhao, C. Y. Experimental study of CaO/Ca(OH)2 in a fixed-bed reactor for thermochemical heat storage. *Appl. Energy* **2016**, *175*, 277−284.

(3) Kim, Y.; Kim, N.; Kim, T. S.; Park, G. J.; Kwon, Y.; Yu, H. K. Mg(OH)2 nano-sheet decorated MgO micro-beams by electron beam irradiation for thermochemical heat storage. *Ceram. Int.* **2019**, *45* (15), 18908−18913.

(4) Zhong, Y.; Critoph, R. E.; Thorpe, R. N.; Tamainot-Telto, Z.; Aristov, Y. I. Isothermal sorption characteristics of the BaCl2−NH3 pair in a vermiculite host matrix. *Appl. Therm. Eng.* **2007**, *27* (14−15), 2455−2462.

(5) Cosquillo Mejia, A.; Afflerbach, S.; Linder, M.; Schmidt, M. Experimental analysis of encapsulated CaO/Ca(OH)2 granules as thermochemical storage in a novel moving bed reactor. *Appl. Therm. Eng.* **2020**, *169*, No. 114961.

(6) N'Tsoukpoe, K. E.; Kuznik, F. A reality check on long-term thermochemical heat storage for household applications. *Renewable Sustainable Energy Rev.* **2021**, *139*, No. 110683.

(7) Li, M.; Lin, Z.; Sun, Y.; Wu, F.; Xu, T.; Wu, H.; Zhou, X.; Wang, D.; Liu, Y. Preparation and characterizations of a novel temperature-tuned phase change material based on sodium acetate trihydrate for improved performance of heat pump systems. *Renewable Energy* **2020**, *157*, 670−677.

(8) N'Tsoukpoe, K. E.; Schmidt, T.; Rammelberg, H. U.; Watts, B. A.; Ruck, W. K. L. A systematic multi-step screening of numerous salt hydrates for low temperature thermochemical energy storage. *Appl. Energy* **2014**, *124*, 1−16.

(9) Meesenburg, W.; Markussen, W. B.; Ommen, T.; Elmegaard, B. Optimizing control of two-stage ammonia heat pump for fast regulation of power uptake. *Appl. Energy* **2020**, *271*, No. 115126.

(10) Guo, J.; Huai, X.; Xu, M. Study on Isopropanol−Acetone−Hydrogen chemical heat pump of storage type. *Sol. Energy* **2014**, *110*, 684−690.

(11) Li, S.; Huang, H.; Yang, X.; Bai, Y.; Li, J.; Kobayashi, N.; Kubota, M. Hydrophilic substance assisted low temperature LiOH·H2O based composite thermochemical materials for thermal energy storage. *Appl. Therm. Eng.* **2018**, *128*, 706−711.

(12) Myat, A.; Kim Choon, N.; Thu, K.; Kim, Y.-D. Experimental investigation on the optimal performance of Zeolite−water adsorption chiller. *Appl. Energy* **2013**, *102*, 582−590.

(13) Thao Ho, T. T.; Zimmermann, T.; Caseri, W. R.; Smith, P. Liquid ammonia treatment of (cationic) nanofibrillated cellulose/vermiculite composites. *J. Polym. Sci., Part B: Polym. Phys.* **2013**, *51* (8), 638−648.

(14) Shrungi, M.; Goswami, A.; Bajpai, J.; Bajpai, A. K. Designing kaolin-reinforced bionanocomposites of poly(vinyl alcohol)/gelatin and study of their mechanical and water vapor transmission behavior. *Polym. Bull.* **2019**, *76* (11), 5791−5811.

(15) Lin, K.-L.; Lee, T.-C.; Chang, J.-C.; Lan, J.-Y. Water absorption and retention of porous ceramics cosintered from waste diatomite and catalyst. *Environ. Prog. Sustainable Energy* **2013**, *32* (3), 640−648.

(16) Krajnc, A.; Varlec, J.; Mazaj, M.; Ristić, A.; Logar, N. Z.; Mali, G. Superior Performance of Microporous Aluminophosphate with LTA Topology in Solar-Energy Storage and Heat Reallocation. *Adv. Energy Mater.* **2017**, *7* (11), No. 1601815, DOI: 10.1002/aenm.201601815.

(17) Akiyama, G.; Matsuda, R.; Sato, H.; Hori, A.; Takata, M.; Kitagawa, S. Effect of functional groups in MIL-101 on water sorption behavior. *Microporous Mesoporous Mater.* **2012**, *157*, 89−93.

(18) Solovyeva, M. V.; Aristov, Y. I.; Gordeeva, L. G. NH 2 -MIL-125 as promising adsorbent for adsorptive cooling: Water adsorption dynamics. *Appl. Therm. Eng.* **2017**, *116*, 541−548.

(19) Hu, Y.; Xiang, S.; Zhang, W.; Zhang, Z.; Wang, L.; Bai, J.; Chen, B. A new MOF-505 analog exhibiting high acetylene storage. *Chem. Commun.* **2009**, No. 48, 7551−7553.

(20) Ehrenmann, J.; Henninger, S. K.; Janiak, C. Water Adsorption Characteristics of MIL-101 for Heat-Transformation Applications of MOFs. *Eur. J. Inorg. Chem.* **2011**, *2011* (4), 471−474.

(21) Khutia, A.; Rammelberg, H. U.; Schmidt, T.; Henninger, S.; Janiak, C. Water Sorption Cycle Measurements on Functionalized MIL-101Cr for Heat Transformation Application. *Chem. Mater.* **2013**, *25* (5), 790−798.

(22) Akiyama, G.; Matsuda, R.; Kitagawa, S. Highly Porous and Stable Coordination Polymers as Water Sorption Materials. *Chem. Lett.* **2010**, *39* (4), 360−361.

(23) Wu, Y.-t.; Ren, N.; Wang, T.; Ma, C.-f. Experimental study on optimized composition of mixed carbonate salt for sensible heat storage in solar thermal power plant. *Sol. Energy* **2011**, *85* (9), 1957−1966.

(24) Donkers, P. A. J.; Pel, L.; Adan, O. C. G. Experimental studies for the cyclability of salt hydrates for thermochemical heat storage. *J. Energy Storage* **2016**, *5*, 25−32.

(25) Yu, N.; Wang, R. Z.; Wang, L. W. Theoretical and experimental investigation of a closed sorption thermal storage prototype using LiCl/water. *Energy* **2015**, *93*, 1523−1534.
(26) Courbon, E.; D'Ans, P.; Permyakova, A.; Skrylnyk, O.; Steunou, N.; Degrez, M.; Frère, M. Further improvement of the synthesis of silica gel and CaCl2 composites: Enhancement of energy storage density and stability over cycles for solar heat storage coupled with space heating applications. *Sol. Energy* **2017**, *157*, 532−541.
(27) Brancato, V.; Calabrese, L.; Palomba, V.; Frazzica, A.; Fullana-Puig, M.; Solé, A.; Cabeza, L. F. MgSO4·7H2O filled macro cellular foams: An innovative composite sorbent for thermo-chemical energy storage applications for solar buildings. *Sol. Energy* **2018**, *173*, 1278−1286.
(28) Garzón-Tovar, L.; Pérez-Carvajal, J.; Imaz, I.; Maspoch, D. Composite Salt in Porous Metal-Organic Frameworks for Adsorption Heat Transformation. *Adv. Funct. Mater.* **2017**, *27* (21), No. 1606424, DOI: 10.1002/adfm.201606424.
(29) Sun, Y.; Spieß, A.; Jansen, C.; Nuhnen, A.; Gökpinar, S.; Wiedey, R.; Ernst, S.-J.; Janiak, C. Tunable LiCl@UiO-66 composites for water sorption-based heat transformation applications. *J. Mater. Chem. A* **2020**, *8* (26), 13364−13375.
(30) Yan, J.; Yu, Y.; Ma, C.; Xiao, J.; Xia, Q.; Li, Y.; Li, Z. Adsorption isotherms and kinetics of water vapor on novel adsorbents MIL-101(Cr)@GO with super-high capacity. *Appl. Therm. Eng.* **2015**, *84*, 118−125.
(31) Oh, J. S.; Shim, W. G.; Lee, J. W.; Kim, J. H.; Moon, H.; Seo, G. Adsorption Equilibrium of Water Vapor on Mesoporous Materials. *J. Chem. Eng. Data* **2003**, *48* (6), 1458−1462.
(32) de Lange, M. F.; Verouden, K. J.; Vlugt, T. J.; Gascon, J.; Kapteijn, F. Adsorption-Driven Heat Pumps: The Potential of Metal-Organic Frameworks. *Chem. Rev.* **2015**, *115* (22), 12205−12250.
(33) Jeremias, F.; Khutia, A.; Henninger, S. K.; Janiak, C. MIL-100(Al, Fe) as water adsorbents for heat transformation purposes—a promising application. *J. Mater. Chem.* **2012**, *22* (20), 10148−10151.
(34) Zhao, Y. J.; Wang, R. Z.; Zhang, Y. N.; Yu, N. Development of SrBr2 composite sorbents for a sorption thermal energy storage system to store low-temperature heat. *Energy* **2016**, *115*, 129−139.
(35) Ferey, G.; Mellot-Draznieks, C.; Serre, C.; Millange, F.; Dutour, J.; Surble, S.; Margiolaki, I. A Chromium Terephthalate-Based Solid with Unusually Large Pore Volumes and Surface Area. *Science* **2005**, *309* (5743), 2040−2042.
(36) Whiting, G. T.; Grondin, D.; Stosic, D.; Bennici, S.; Auroux, A. Zeolite−MgCl2 composites as potential long-term heat storage materials: Influence of zeolite properties on heats of water sorption. *Sol. Energy Mater. Sol. Cells* **2014**, *128*, 289−295.
(37) Balula, S. S.; Granadeiro, C. M.; Barbosa, A. D. S.; Santos, I. C. M. S.; Cunha-Silva, L. Multifunctional catalyst based on sandwich-type polyoxotungstate and MIL-101 for liquid phase oxidations. *Catal. Today* **2013**, *210*, 142−148.
(38) Ren, J.; Dyosiba, X.; Musyoka, N. M.; Langmi, H. W.; North, B. C.; Mathe, M.; Onyango, M. S. Green synthesis of chromium-based metal-organic framework (Cr-MOF) from waste polyethylene terephthalate (PET) bottles for hydrogen storage applications. *Int. J. Hydrogen Energy* **2016**, *41* (40), 18141−18146.
(39) Zhang, D.; Zhang, K.; Hu, X.; He, Q.; Yan, J.; Xue, Y. Cadmium removal by MgCl2 modified biochar derived from crayfish shell waste: Batch adsorption, response surface analysis and fixed bed filtration. *J. Hazard Mater.* **2021**, *408*, No. 124860.
(40) Yang, X.; Shen, L.; Yang, Q.; Wang, K.; Wang, C. Study on the synthesis and thermal properties of magnesium chloride hexahydrate−magnesium sulfate heptahydrate−activated carbon phase change heat storage materials. *Appl. Phys. A: Mater. Sci. Process.* **2021**, *127* (8), No. 578, DOI: 10.1007/s00339-021-04675-7.
(41) Jeremias, F.; Lozan, V.; Henninger, S. K.; Janiak, C. Programming MOFs for water sorption: amino-functionalized MIL-125 and UiO-66 for heat transformation and heat storage applications. *Dalton Trans.* **2013**, *42* (45), 15967−15973.
(42) Stefan, K.; Henninger, H. A. H.; Janiak, C. MOFs as Adsorbents for Low Temperature Heating and Cooling Applications. *J. Am. Chem. Soc.* **2009**, *131* (8), 2776−2777, DOI: 10.1021/ja808444z.
(43) Kummer, H.; Baumgartner, M.; Hügenell, P.; Fröhlich, D.; Henninger, S. K.; Gläser, R. Thermally driven reflection by metal adsorption on coatings of HKUST-1 and MIL-101 (Cr). *Appl. Therm. Eng.* **2017**, *117*, 689−697, DOI: 10.1016/j.applthermaleng.2016.11.026.
(44) Ait Ousaleh, H.; Sair, S.; Zaki, A.; Faik, A.; Mirena Igartua, J.; El Bouari, A. Double hydrates salt as sustainable thermochemical energy storage materials: Evaluation of dehydration behavior and structural phase transition reversibility. *Sol. Energy* **2020**, *201*, 846−856, DOI: 10.1016/j.solener.2020.03.067.

https://doi.org/10.1021/acsomega.3c06004
ACS Omega 2024, 9, 509−519